J Physiol Sci (2011) 61:445–456
DOI 10.1007/s12576-011-0164-9

ORIGINAL PAPER

Responses of HSC70 expression in diencephalon to iron deficiency anemia in rats

Fuminori Kawano · Yoshihiko Oke · Sachiko Nomura · Ryo Fujita · Takashi Ohira · Naoya Nakai · Yoshinobu Ohira

Received: 25 April 2011 / Accepted: 6 July 2011 / Published online: 3 August 2011

Abstract A powdered diet containing 100 or 3 ppm Fe was fed to rats starting at the age of 3 weeks. The voluntary activity level was checked using a wheel in the cage during the 17th week after the beginning of supplementation. Significantly less activity was seen in the 3 ppm Fe group during both light and dark periods. After 20 weeks, the blood and diencephalon were sampled from both groups. Lower hematocrit and blood hemoglobin content was observed in the 3 ppm Fe group. The level of 70 kDa heat shock cognate (HSC70) expression was greater in the diencephalon of the 3 ppm Fe group. In addition, the distribution of HSC70 was determined by proximity ligation assay. More HSC70-positive as well as total cells were noted in several areas of the diencephalon of the iron-deficient rats. The altered expression and distribution of HSC70 might play some role in the neurological changes.

Keywords Iron deficiency anemia · Rat diencephalon · Proteomics · Proximity ligation assay · 70 kDa heat shock cognate

Introduction

Dietary iron deficiency causes anemia and results in decreased work performance in humans [1–3] and rats [4–10]. Iron is also known as the essential molecule for proper neurogenesis and differentiation of certain brain cells and regions [11–13]. It was further reported that decreased dietary availability of iron is associated with hypomyelination in rat brain [14, 15]. In human studies, iron-deficient children showed the common neurological signs, such as poor school performance, decreased cognitive abilities, and behavior problems [16–18]. These neurological abnormalities remained even after therapeutic supplementation of iron [19–21]. However, the precise mechanisms responsible for iron deficiency-induced neuropathology are still unclear.

The thalamus is located within the diencephalon and is known as the entryway for incoming sensorimotor information to the cerebral cortex and the locus of efferent influences from both basal ganglia and neocortex on the behavioral outputs [22, 23]. The synaptic changes in the thalamic nuclei represent a potentially important component in psychomotor sensitization and addiction [24]. Further, it was reported that the connections between the hypothalamus and medial prefrontal cortex largely contribute to the behavioral and autonomic functions in rats [25–27]. These facts may indicate that the diencephalon plays an important role in behavior of mammals. However, few in vivo studies have been performed to investigate the organic changes or cellular mechanisms in the diencephalon of iron-deficient and anemic rats. Since the present study focused on the effects of iron deficiency anemia on the psychomotor system in rats, the diencephalon was targeted in this manuscript.

Advanced proteome analysis is a powerful tool for studying cellular mechanisms and finding new insights into pathology. Recent studies have identified the proteins expressed in the brain of Alzheimer's [28–30] and Parkinsons's [31–33] disease and dementia with Lewy bodies

F. Kawano · Y. Oke · S. Nomura · R. Fujita · N. Nakai · Y. Ohira (✉)
Section of Applied Physiology, Graduate School of Medicine, Osaka University, Toyonaka, Osaka 560-0043, Japan
e-mail: ohira@space.hss.osaka-u.ac.jp

T. Ohira · Y. Ohira
Graduate School of Frontier Biosciences, Osaka University, Toyonaka, Osaka 560-0043, Japan

[32, 34] in humans. Therefore, the proteomic approach was performed to study the possible factor(s) related to the neurological changes in the diencephalon of iron-deficient and anemic rats in the present investigation.

Materials and methods

Animal care and experimental model

All experimental procedures were conducted in accordance with the Japanese and American Physiological Society *Guide for the Care and Use of Laboratory Animals*. The study was also approved by the Animal Use Committee at Osaka University.

Male Wistar Hannover rats (Nihon CREA, Tokyo) were randomly separated into the control (100 ppm Fe, $n = 7$) and iron-deficient (3 ppm Fe, $n = 7$) groups at the age of 3 weeks. The powdered diet containing 100 or 3 ppm Fe (Nihon CREA) was fed to the respective groups for 20 weeks. The original diet, which was composed of 61% cornstarch, 22% milk casein, 7% mineral mixture, 5% crystallized cellulose, 4% purified soybean oil, and 1% vitamin mixture, contained 100 ppm Fe, but 0.058% $FeC_6H_5O_7{\cdot}5H_2O$ was replaced with 0.058% cornstarch to adjust the iron content to 3 ppm. Two or three rats were housed in the same cage (45 × 28 cm and 20-cm height). The amount of food provided during the first week of the experiment was increased gradually. From week 4 to the end of experiment, 20 g of food, which was completely eaten within a day, was supplied to each rat per day. Distilled water was also given to both groups ad libitum. Temperature and humidity in the animal room were maintained at ~23°C and ~55%, respectively, with a 12:12 h light:dark cycle.

Voluntary activity

During the 17th week after the beginning of the experiment, voluntary activity was determined. Each rat was assigned individually to a cage (40 × 15 × 14 cm) equipped with a running wheel (10 cm wide and 37 cm diameter, Shinano), thereby permitting the rat to run voluntarily. The recording was started at 3 p.m. and continued for 24 h. The total number of wheel revolutions was registered every 1 h using the connected printer with a counter (Shinano). The total numbers during the light (3–6 p.m. on the first day and 6 a.m.–3 p.m. the next day) and dark (6 p.m. on the first day to 6 a.m. the next day) periods, as well as the total daily activity level, were calculated for each rat. During the whole-day recording, 20 g of food was supplied to each cage. Distilled water was also given ad libitum.

Tissue sampling and preparation for proteomic and histochemical analyses

After 20 weeks, the rats in both groups were anesthetized by i.p. injection of sodium pentobarbital (5 mg/100 g body weight). Blood was withdrawn into a heparin-coated syringe from the jugular vein before the sampling of the brain ($n = 4$ in each group). The diencephalon was isolated from the sampled brain and frozen in liquid nitrogen. Subsequently, the frozen diencephalon was powdered in a liquid nitrogen-cooled mortar and dissolved in the lysis buffer (1% triton X-100, 20 mM Tris, 150 mM sodium chloride, 50 mM sodium fluoride, and 1 mM sodium vanadate, pH 7.6) overnight at 4°C. On the next day, the dissolvent was centrifuged at 1,200*g* for 10 min, and the supernatant was saved and stored at −80°C until analyses. Furthermore, the crude extract of four rats was mixed (1 mg protein per rat × 4), and the extract containing 4 mg protein in each group was utilized for the fractionation of phosphoproteins using Phosphocruz™ Protein Purification System (Santa Cruz Biotechnology). The obtained phosphoprotein-enriched fraction was also stored at −80°C until analyses.

The remaining rats ($n = 3$ in each group) were perfused by 4% paraformaldehyde diluted in 0.1 M phosphate buffer, and the brain was removed and kept in 4% paraformaldehyde diluted in 0.1 M phosphate buffer overnight at 4°C. The fixed brains were further placed in 30% sucrose diluted in 0.1 M phosphate buffer overnight at 4°C. Then, the brain was frozen in isopentane cooled to −80°C. The cerebrum was mounted on a cork by using OCT (optimum cutting temperature) compound (Miles) for the histochemical analyses of the cross-sections.

Hematocrit and hemoglobin content

Hematocrit levels were analyzed by centrifugation of capillary tubes filled with blood at 11,000 rpm for 5 min using a high-speed hematocrit centrifuge (Kubota). Further, the remaining blood was dissolved in 200 parts of hemolysis solution containing 0.02% potassium hexacyanoferrate (III), 0.005% potassium cyanide, and 0.1% sodium hydrogen carbonate. The absorbance at 540 nm was measured using the spectrometry (SmartSpec™ Plus, Bio-Rad). The hemoglobin content (g/dL) was then calculated (the absorbance × 0.146 coefficient × 200, where 200 is the dilution factor).

Two-dimensional electrophoresis

The crude extract of diencephalon containing 25 μg protein was made for each group by mixing an equal amount of protein (6.25 μg/rat × 4 rats), desalted and precipitated using 2-D Clean-Up kit (GE Healthcare). The whole

amount of phosphoprotein-enriched fraction obtained from the crude extract containing 4 mg protein was also desalted and precipitated. The precipitate was dissolved in 150 μL DeStreak rehydration solution containing 0.5% IPG buffer (pH 3–10, GE Healthcare). The dissolvent, containing the protein, was absorbed in the dry-strip gel with the pH gradient 3–10 (7 cm length, GE Healthcare) for 12 h. Subsequently, the isoelectric focusing was performed using IPGphor^{TM} system (GE Healthcare). The voltage was gradually increased from 500 to 5,000 V keeping the current constant at 100 μA. The gels were then washed in pure water for 2 h and incubated in the equilibrating buffer [6 M urea, 2% sodium dodecylsulfate (SDS), 30% glycerol, and 50 mM Tris-HCl, pH 8.7] containing 1% dithiothreitol or 2.5% iodoacetamide for 15 min at room temperature. Further, SDS-polyacrylamide gel electrophoresis (PAGE) was carried out on 10% polyacrylamide slab gel with 1 mm thickness keeping the current constant at 10 mA per gel for ~3 h at 4°C. After two-dimensional electrophoresis (2DE), the gels for the crude extract were silver-stained using SilverQuest^{TM} silver staining kit (Invitrogen), whereas the gels for the phosphoprotein-enriched fraction were stained using the staining solution containing 2% coomassie brilliant blue (CBB), 40% methanol, and 10% acetic acid for 15 min. After the CBB staining, the stained gels were washed in the solution containing 20% methanol and 5% acetic acid for 6 h. The stained gels were then computerized using a gel image scanner (GE Healthcare) to compare the spot pattern between the 100 ppm and 3 ppm Fe groups.

Peptide mass fingerprint

Spots with differences in the expression levels (spots in the dotted circles of Fig. 3b) were sampled, destained in the destaining solution (50 mM ammonium hydrogen carbonate and 50% methanol) at 40°C, and ground into small pieces using a pestle. The gel pieces were then dried using the centrifugal concentrator (Taitec), rehydrated in 50 mM Tris-HCl buffer (pH 8.7) containing 5 μM trypsin (Promega), and incubated overnight at 37°C. The peptide fragments were collected, concentrated using the centrifugal concentrator, and desalted using ZipTip C18 (Millipore). Ultraflex mass spectrometry (Bulker Daltonics) was used to obtain the mass spectrum of peptide fragments. Subsequently, a database search on the MCBI web site was performed using the obtained mass of peptides.

Western blot

The crude extract was dissolved in an equal volume of 2× SDS sample buffer (20% glycerol, 12% 2-mercaptoethanol, 4% SDS, 100 mM Tris-HCl, and 0.05% bromophenol blue, pH 6.7) and adjusted to the final concentration of 1 μg protein per μL by 1× SDS sample buffer. The SDS-PAGE was carried out on 10% polyacrylamide slab gel with 1.5 mm thickness keeping the current constant at 20 mA per gel for ~1 h at 4°C. Equal amounts of protein (10 μg/10 μL) were loaded into each lane.

After SDS-PAGE, the proteins were transferred to poly vinylidene fluoride membranes (Bio-Rad) by using the trans-blot cell (Bio-Rad) keeping the voltage constant at 60 V for 2 h at 4°C. After the transfer of protein, the membranes were blocked in the blocking buffer [5% non-fat dry milk in 0.1% Tween 20 in Tris-buffered saline (TTBS)] for 1 h. The membranes were incubated overnight at 4°C with anti-70 kDa heat shock cognate protein (HSC70, 1:1,000, Stressgen) diluted in TTBS containing 5% BSA. Blots were then incubated with horseradish peroxidase (HRP)-conjugated secondary antibody to mouse IgG (Cell Signaling Technology) for 30 min. The antibody-bound protein was detected by the chemiluminescence method using the enhanced chemiluminescence plus kit (GE Healthcare). After the first immunoreaction, the blots were incubated in WB stripping solution (Nacalai Tesque) for 4 h at 50°C to dissociate the antibodies from the membrane. The blots were again blocked and incubated with the anti-α-tubulin antibody (1:5,000, Santa Cruz Biotechnology). The blots were further reacted with HRP-conjugated secondary antibody to mouse IgG (Cell Signaling Technology), and the bands were visualized by the same procedure stated above.

Western blot was also performed following 2DE. The crude extract containing 10 μg protein was precipitated, desalted, and dissolved in DeStreak rehydration solution as stated above. 2DE and subsequent Western blot were carried out following the above-mentioned procedures. Quantification of the bands and spots was carried out using image analyzing software (Scion Image). The protein expression level was represented as the integrated density of band or spot, which was calculated as the mean density multiplied by the band area.

Proximity ligation assay

To determine the distribution of HSC70, the magnification of HSC70 signals was performed by proximity ligation assay (PLA) [35, 36] by using a commercial kit (Duolink, Olink Bioscience). The frozen coronal sections in the diencephalon of perfused rats (4 μm thickness) were made approximately 3 mm dorsal from the bregma using a cryostat (Leica Microsystems) maintained at −20°C. The sections were fixed in 0.1 M phosphate buffer containing 4% paraformaldehyde for 10 min and degreased in 100% methanol for 10 min at −20°C. The antigen retrieval was then performed in the target retrieval solution (Dako) for

20 min at 95°C. The sections were permeabilized in the phosphate-buffered saline containing 1% Triton X-100 for 15 min, blocked in 1× blocking buffer (Olink Bioscience) for 30 min at 37°C, and incubated in the mouse monoclonal IgG specific to HSC70 (Stress Marq Bioscience), diluted (1:100) in the antibody diluent (Olink Bioscience) overnight at 4°C.

On the next day, the sites bound with first antibody were further labeled by the oligonucleotide-conjugated antibody specific to the mouse IgG (mouse plus and minus PLA probe, Olink Bioscience), which was diluted (1:10 for each probe) with the antibody diluent (Olink Bioscience) for 2 h at 37°C. Conjugation and ligation of connector oligonucleotide were performed for 1 h for each reaction at 37°C using the kit (Olink Bioscience). Subsequently, the conjugated oligonucleotide was amplified by the DNA polymerase (Olink Bioscience) for 3 h at 37°C. The amplified oligonucleotide was then detected by Texas-red-conjugated DNA probe (Olink Bioscience). The stained sections were mounted in the mounting medium (Olink Bioscience) for the microscopic analysis. The negative control was also tested for the accurate detection of HSC70. The staining of the negative control sections was followed by the same procedures, but the sections were incubated without the primary antibody.

Image analysis

The portion in the stained section was captured digitally with a fluorescent microscope system and CCD camera (BX50 and DP20, OLYMPUS). The numbers of total and HSC70-positive cells were counted in each portion. Percent distribution of HSC70-positive cells relative to the total cells in the portion was also calculated. The number of cells was counted on both the right and left side and averaged. Two sections were measured approximately 3 mm dorsal from the bregma in each rat.

Statistical analyses

All values are expressed as means ± SEM. Significant differences between the 100 ppm and 3 ppm Fe groups were examined by unpaired *t* test. Differences were considered significant at the 0.05 level of confidence.

Results

Voluntary activity

During the 17th week after the beginning of the experiment, the total number of revolutions per day was ~5,200 in the control rats (100 ppm Fe group) (Fig. 1). The number of revolutions in the 3 ppm Fe group was significantly less (−31%, $p < 0.05$) than the controls. The rats in the 3 ppm Fe group also showed significantly less voluntary activity during the light (−29%) and dark (−33%) period compared with the control rats ($p < 0.05$).

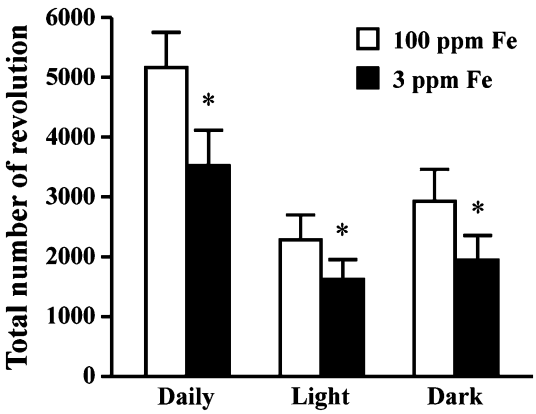

Fig. 1 Voluntary activity levels of rats in 100 ppm (*open bars*) and 3 ppm (*solid bars*) Fe groups. Total revolutions of the running wheel per day were measured during the 17th week after the beginning of experiment. The numbers of revolutions in the light and dark periods were also calculated. Mean ± SEM. *$p < 0.05$ versus 100 ppm Fe group

Body weight and hematology

No significant difference was observed in the body weight between the 100 and 3 ppm Fe groups after the 20 week experiment (Fig. 2a). The mean hematocrit level in the 100 ppm Fe group was approximately 45%, and that in the 3 ppm Fe group was only 17% ($p < 0.05$, Fig. 2b). The blood hemoglobin concentration was also ~73% less in the rats of the 3 ppm Fe group (4.1 g/dL) than the control group (15.0 g/dL) ($p < 0.05$, Fig. 2c).

2DE and peptide mass fingerprint

The 2DE gel spots, visualized by silver staining, are shown in Fig. 3a. Up- or down-regulation of the spot intensity was not clearly seen in response to the provision of low-iron diet. Figure 3b shows the magnified images of the 2DE gel spots in the phosphoproteins stained by CBB. The expression intensity of spots enclosed by the broken circles seemed to be greater in the 3 ppm Fe group than in the control. In addition, the density of the most acidic spot (arrowheads in Fig. 3b) was remarkably higher in the 3 ppm Fe compared with the 100 ppm Fe group.

The spots enclosed by the dotted circles in Fig. 3b were sampled and combined, and the proteins in the spots were determined by the peptide mass fingerprint. The obtained mass spectrum of the peptide fragments is shown in

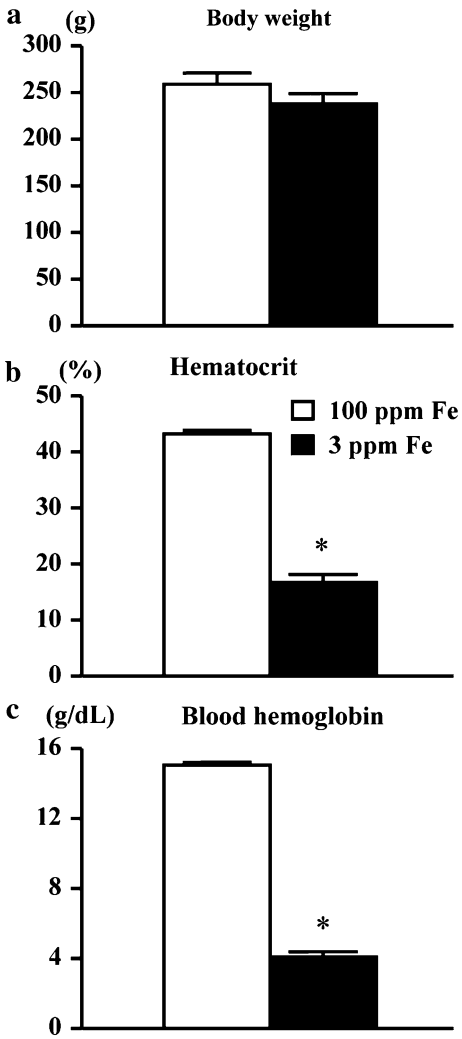

Fig. 2 Body weight (**a**), hematocrit (**b**), and blood hemoglobin concentration (**c**) after 20 week provision of 100 ppm (*open bars*) and 3 ppm (*solid bars*) Fe diet. Mean ± SEM. *$p < 0.05$ versus 100 ppm Fe group

Fig. 4a. In this spectrum, 39 peaks with different masses were detected (Fig. 4b). According to the results of the MASCOT search, the scores (greater than 60) of six proteins were significant (Fig. 4c). The heat shock protein 8 (70 kDa heat shock cognate protein, HSC70) was identified in five out of six matched proteins (nos. 1–4 and 6 of the list shown in Fig. 4c). Figure 4d shows the amino acid sequence of HSC70, and 34.5% of the full sequence of HSC70 was detected based on the peptide mass, shown using red in Fig. 4b.

Expression of HSC70

The expression level of HSC70 was quantified by Western blot. The total HSC70 level was significantly greater (+89%) in the 3 ppm than the 100 ppm Fe group (Fig. 5a, b). No difference was seen in the level of α-tubulin, which was the internal control of the homogenate (Fig. 5a). Five spots were detected as HSC70 by Western blot following 2DE (spots a–e in Fig. 5c). The intensity of each spot was not affected by the provision of the low iron diet (Fig. 5d).

Distribution of HSC70

Figure 6 shows the typical staining patterns following PLA in rat diencephalon. Generally, red signals following PLA were observed in the cell bodies and the extracellular space in which nerve fibers and interstitial space were thought to be exist. The major distribution of cells with the intracellular expression of HSC70 was in the medial region of the diencephalon, such as the medial habenular nucleus (MH), post paraventricular thalamic nucleus (PVP), central medial thalamic nucleus (CM), and ventromedial hypothalamic nucleus (VMH), whereas the higher density of PLA signals was observed in the extracellular space of the lateral region, such as the internal capsule (ic, Fig. 6b). The PLA signal aggregates were also noted in the extracellular space of the regions close to ic, such as the ventral posteromedial thalamic nucleus (VPM) and ventral posterolateral thalamic nucleus (VPL), as well as the mammillothalamic tract (mt). Non-specific staining was not observed in the negative control, in which the sections were incubated without the primary antibody (data not shown).

The number of total and HSC70-positive cells was counted, and the percent distribution was calculated in the mediodorsal thalamic nucleus (MDC, Fig. 7a–c), VPM (Fig. 7d–f), VPL (Fig. 7g–i), ventromedial thalamic nucleus (VM, Fig. 7j–l), and mt (Figs. 7m–o, 8) of the 100 ppm and 3 ppm Fe groups. The middle portion, including MH, PVP, CM, and VMH, was omitted from the analysis, since most of the cells expressed HSC70 in this portion of the 100 ppm and 3 ppm Fe groups. In contrast, the distribution of HSC70-positive cells was minor in ic of both the 100 ppm and 3 ppm Fe groups. Therefore, this portion was also omitted from the analysis. The numbers of both total and HSC70-positive cells in the MDC, VPL, VM, and mt regions were greater in the 3 ppm than the 100 ppm Fe group ($p < 0.05$), whereas no significant effects of iron levels were seen in the percent distribution (Fig. 7). No significant effects on the distribution of these cells were induced in the VPM region following the provision of low-iron diet (Fig. 7d–f).

Discussion

It has been reported that iron-deficient children show common neurological signs, such as poor school performance, decreased cognitive abilities, and behavior problems [16–18]. However, the precise mechanisms

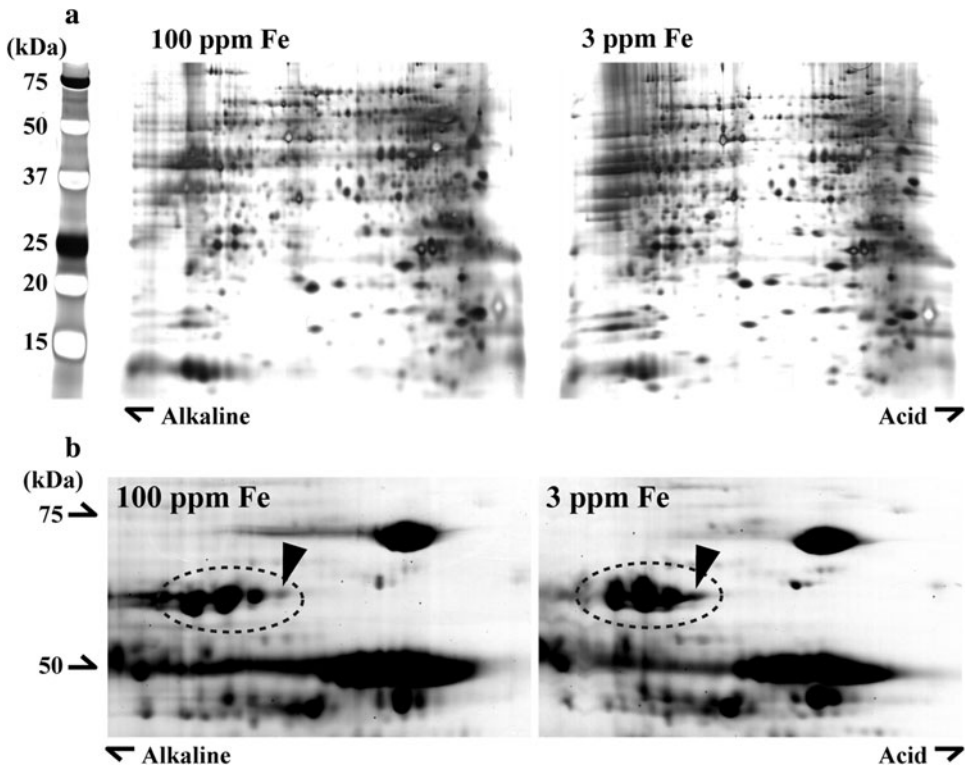

Fig. 3 Gel images following two-dimensional electrophoresis (2DE) in the crude extract (**a**) and the phosphoprotein-enriched fraction (**b**). No spots with clear differences in expression were observed in the gels following 2DE using the crude extract (**a**). However, the expression intensity of the spots enclosed by the *dotted circles* seemed to be greater in the 3 ppm than in the 100 ppm Fe group (**b**). Further, the density of the most acidic spot (*arrowheads*) was remarkably higher in the 3 ppm compared with the 100 ppm Fe group

responsible for the iron deficiency-related neuropathology are still unclear. Here we report that greater HSC70 expression and/or increased number of HSC70-positive cells in the brain might be one of the possible neuropathological factors related to iron deficiency anemia.

Effects of iron deficiency on physical parameters

The provision of a low-iron diet, containing 3 ppm Fe, caused anemia, as was also reported previously [4, 8, 10]. However, weight gain was not affected by the iron deficiency and anemia. A lower voluntary activity level was seen in the iron-deficient rats in the present study. The data agreed with the previous study, which reported that rats with iron deficiency and anemia performed fewer revolutions in the voluntary wheel running [37]. These observations indicated that the iron deficiency and anemia inhibited daily voluntary activity in rats. The water-maze test was also performed in the same experimental series, but no differences were seen in the time and distance to the platform between the 100 ppm and 3 ppm Fe groups (data not shown). The result suggested that iron deficiency anemia in rats does not affect the learning capability and cognitive function.

HSC70 expression in brain

Greater expression of HSC70 was observed in the diencephalon of rats with iron deficiency anemia in the present study. According to the staining intensity in Fig. 3b, it was speculated that the level of phosphorylation might be altered. But the speculation was not correct, although the total expression was increased. Therefore, it was suggested that the iron deficiency anemia did not contribute to the phosphorylation-associated functional changes in HSC70 in the brain.

The constitutively expressed HSC70 and heat-inducible 72 kDa heat shock protein (HSP72) belong to the 70 kDa family of HSPs in brain [38, 39]. The increased expression of HSC70 was previously found in the Lewy bodies of the brain in humans with a clinical history of dementia [32] or Parkinson's disease [38]. Increased HSC70 was co-localized with α-synuclein, which is known as the major component of Lewy bodies in the Parkinsonian midbrain, suggesting that HSC70 inhibits the aggregation of aberrant protein by its chaperoning function [38]. Therefore, the increased expression of HSC70 indicates the abnormality of neurons and/or glial cells in the diencephalon of iron-deficient and anemic rats.

Furthermore, there is a possibility that one of the causes for lower HSC70 expression in the iron-deficient rats might be the inhibited daily activity indicated by the wheel running test. Sumitani et al. [40] reported that HSC70 level in the hippocampus of mice was increased following severe long-term exercise. In contrast, Chen et al. [41] reported that the level of HSC70 in the hippocampus of rats did not change in response to voluntary or forced (treadmill) exercise performed from the age of 5 months to 23 months.

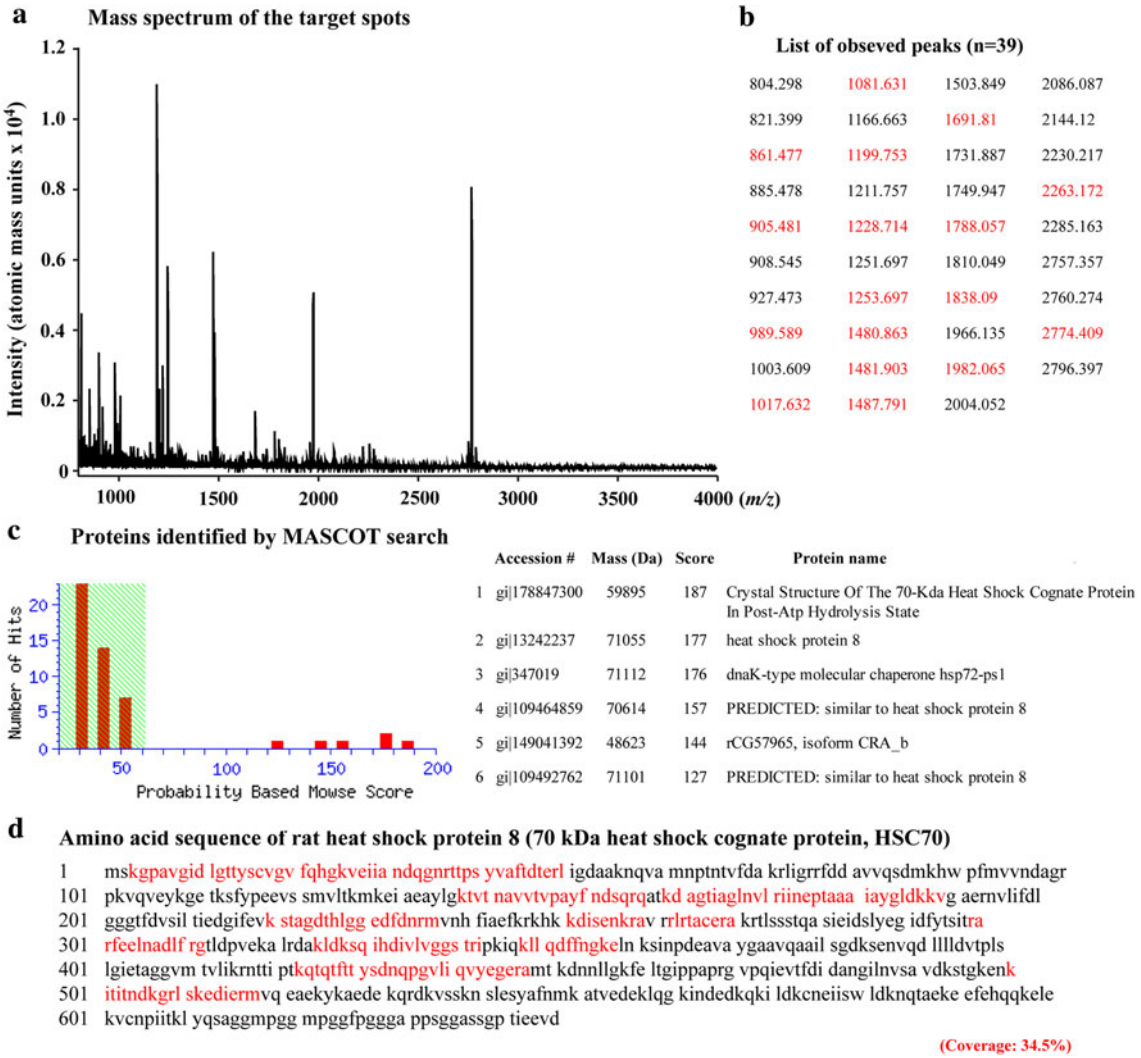

Fig. 4 **a** Mass spectrum of the peptide fragments analyzed in the spots enclosed by *dotted circles* in Fig. 3b. **b** List of peaks seen in the spectrum. Thirty-nine peaks were detected. The *peaks* indicated by *red characters* were matched with the protein sequences listed in **c**. **c** Results of the NCBI database search. The distributions (numbers) of the scores of 44 proteins, shown by the *three bars* on the *left side*, were not significant. But those of six proteins with scores higher than 60 were significant. The names of those proteins are listed on the *right*. Five (nos. 1–4 and 6) out of six proteins were identified as heat shock protein 8 (70 kDa heat shock cognate protein, HSC70). **d** Full amino acid sequence of HSC70. The sequences estimated by the peptide mass, which are also indicated in **b**, are shown as *red characters*. A total of 34.5% of the full sequence of HSC70 was detected by the peptide mass, shown in *red* in **b**

Therefore, it is still unclear whether the daily activity level is related to the change in the expression of HSC70 in brain.

It was further reported that HSC70 was necessary for the optimal synthesis of myelin basic protein in the oligodendrocytes during differentiation [42]. Oligodendrocytes are one of the glial cells that produce myelin [15]. Iron is known as the differentiation marker of the oligodendrocytes [14, 15]. Badaracco et al. [14] reported that hypomyelination was induced in the brain of the iron-deficient rat pups, whereas the postnatal treatment of apotransferrin by intracranial injection stimulated myelination. These investigations indicate that HSC70 and iron accumulation are required for the normal differentiation and myelination of the oligodendrocytes. However, the present data showed inhibited daily voluntary activity in iron-deficient and anemic rats with greater expression of HSC70 in the brain. Although the levels of HSC70 and myelination in the oligodendrocytes were not checked in the present study, the differentiation and myelination of the oligodendrocytes may not be the main causes responsible for the behavioral outcome, based on the discrepancy with the results of the previous studies.

Localization and distribution of HSC70

The expression of HSC70 was noted in both cell bodies and the extracellular space (Figs. 6, 7, 8). Furthermore, the

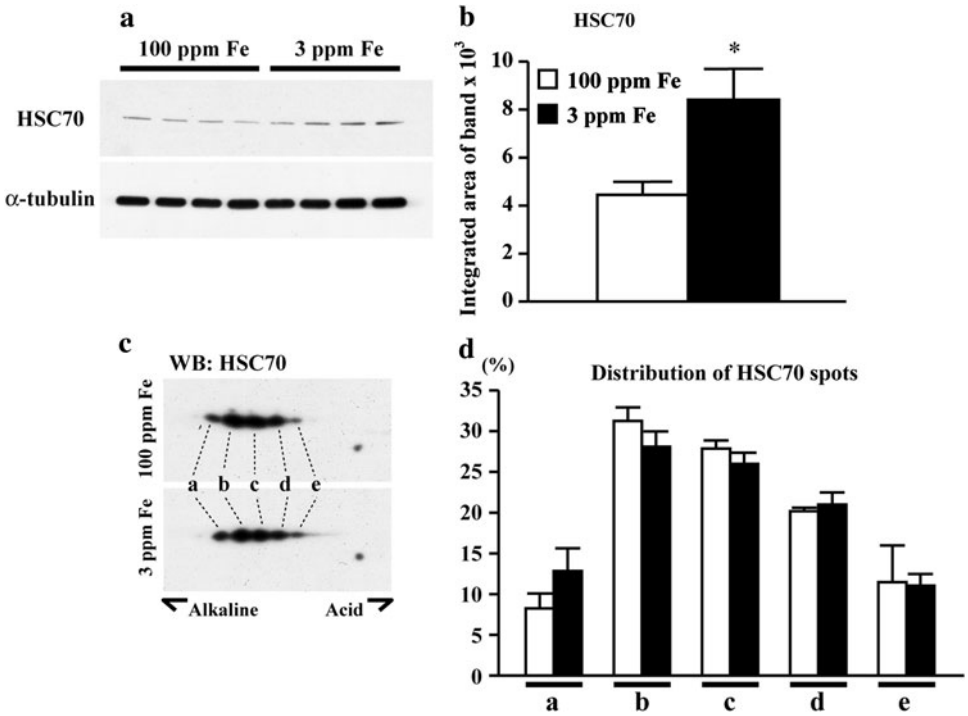

Fig. 5 Western blot analysis of HSC70 expression in the crude extract of diencephalon. **a** Typical blot patterns of HSC70 (*upper*) and α-tubulin (internal control, *lower*). **b** Mean integrated areas of HSC70 bands. **c** Spots detected by Western blot using anti-HSC70 antibody following two-dimensional electrophoresis in the crude extract. Five spots (*a–e*) with different isoelectric points were detected in both the 100 ppm (*upper*) and 3 ppm (*lower*) Fe groups. **d** Mean percent integrated area (density × area) of each spot, relative to the whole five spots (*a–e*), in the 100 ppm (*open bars*) and 3 ppm (*solid bars*) Fe groups. Mean ± SEM. *$p < 0.05$ versus 100 ppm Fe group

PLA signals in the extracellular space were dense in the lateral region of the diencephalon (Fig. 6). However, the type of cells that expressed HSC70 in the cell bodies was not determined.

A greater number of total cells was observed in several portions of the diencephalon of iron-deficient and anemic rats (Fig. 7). More HSC70-positive cells were also seen in these rats, although the percentage of these cells relative to the total cells was similar to that in the normal controls. These results indicated that severe iron deficiency anemia induced the morphological alteration of the diencephalon. A growth-related change in the total number of cells was not found in the present study because the size of each region, as well as the brain size itself, was different between the 3- and 23-week-old rats. The number of cells in mt, where the outline of the region was visualized following the HSC70 staining by PLA, was approximately twofold greater in 3-week-old than 23-week-old rats (data not shown). More cells (+ ~ 34% vs. 100 ppm Fe group), however, were noted in the 3 ppm Fe group (Fig. 7m), although the number was less than that in the 3-week-old group (data not shown). Therefore, it was suggested that the enhanced expression of HSC70 in the individual cells, related to the greater cell number, might inhibit the growth-associated withdrawal of diencephalic cells in the iron-deficient and anemic rats. However, the precise mechanisms responsible for the contribution of HSC70 to the survival or death of diencephalic cells are still unclear.

It has been reported that diencephalon plays some role(s) in the somatosensory input to the cerebral cortex [43, 44]. Therefore, it was speculated that some changes in the somatosensory system may be induced by iron deficiency anemia. It was also reported that the VPM, where no changes were induced by iron deficiency anemia, relayed the thalamocortical input derived from the whisker to the cerebral cortex [45, 46]. There might be some region-specific effects of iron deficiency anemia on the somatosensory system. Effects of iron deficiency anemia on the functional properties of each region are still unclear.

Furthermore, the greater expression of HSC70 was noted in the extracellular space of mt, although the morphologies of the signal aggregates were different between the 100 ppm and 3 ppm Fe groups (Fig. 8). For example, the upper picture of the 3 ppm Fe group in Fig. 8 indicated large gap areas between the bundle-like signal aggregates, and there was no clear outline of mt in the lower picture of the 3 ppm Fe group compared with the 100 ppm Fe group. These findings also suggest that morphological changes in the diencephalon may be induced in rats with iron deficiency anemia. Although the precise mechanisms are still unclear, the morphological changes, accompanied by the changes in the expression and distribution of HSC70, might be related to the neuropathogenesis in the brain of iron-deficient and anemic rats. Further studies are needed to investigate the functional responses in each region, as well as the relationship

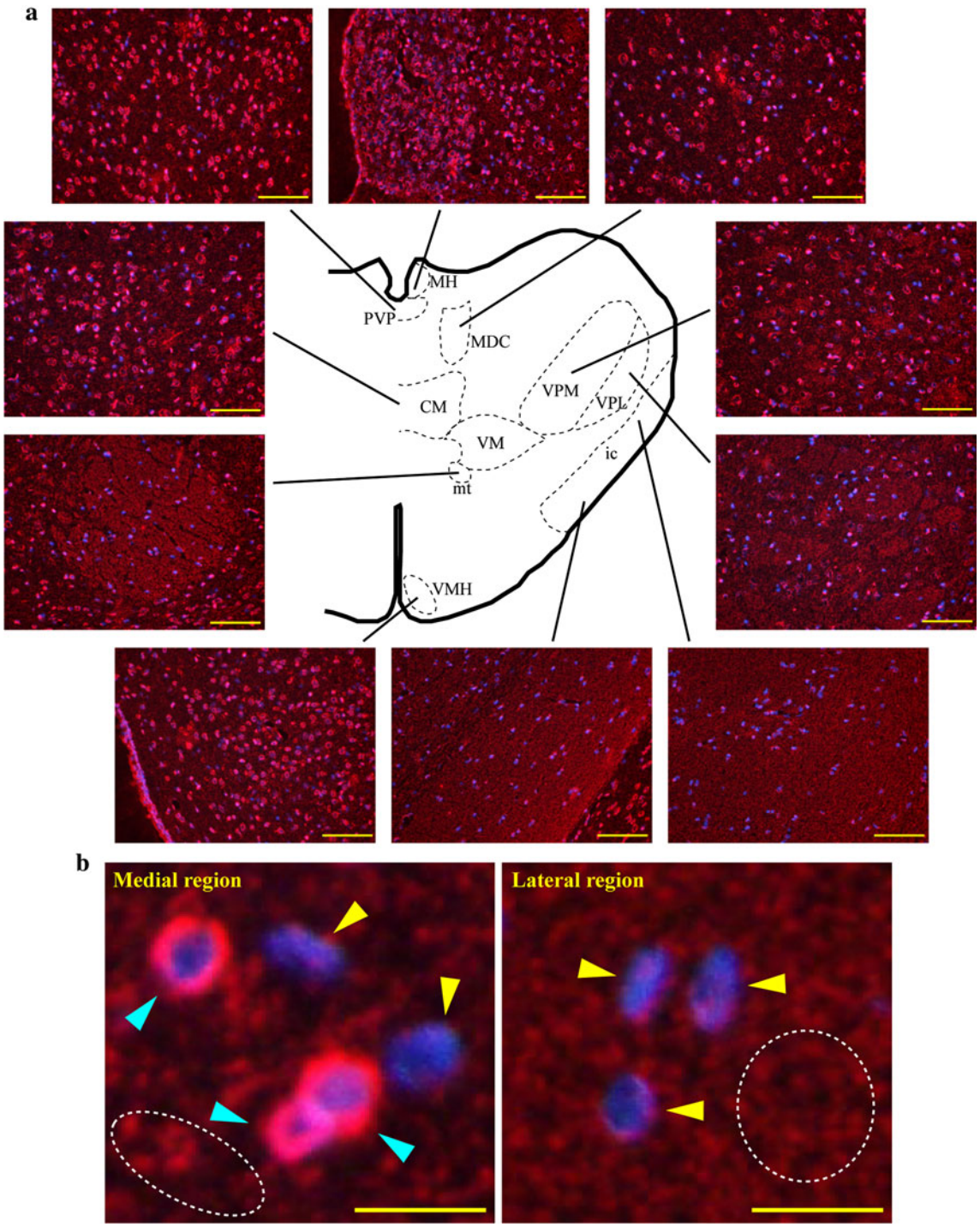

Fig. 6 **a** Typical staining patterns of HSC70 in the particular portions of the rat diencephalon. Immunoreacted signals of HSC70 were amplified by proximity ligation assay (PLA, *red spots*). Nucleus (*blue*), which indicates a single cell, was also labeled by Hoechst33342. Note that the *red signals*, which were detected by PLA, were generally observed in the cell bodies and the extracellular space in which nerve fibers and interstitial space were thought to exist. **b** The magnified images of HSC70-positive (*blue arrowheads*) and HSC70-negative (*yellow arrowheads*) cells in the medial and lateral regions of the diencephalon. The areas enclosed by the *dotted circles* indicate the extracellular space of the diencephalon, in which the PLA signals are also present. Pictures also show the higher intensity of the PLA signals in the extracellular space of the lateral region. *CM* Central medial thalamic nucleus, *ic* internal capsule, *MDC* central mediodorsal thalamic nucleus, *MH* medial habenular nucleus, *mt* mammillothalamic tract, *PVP* post paraventricular thalamic nucleus, *VM* ventromedial thalamic nucleus, *VMH* ventromedial hypothalamic nucleus, *VPL* ventral posterolateral thalamic nucleus, and *VPM* ventral posteromedial thalamic nucleus. *Scale bars* 50 μm (**a**) and 10 μm (**b**)

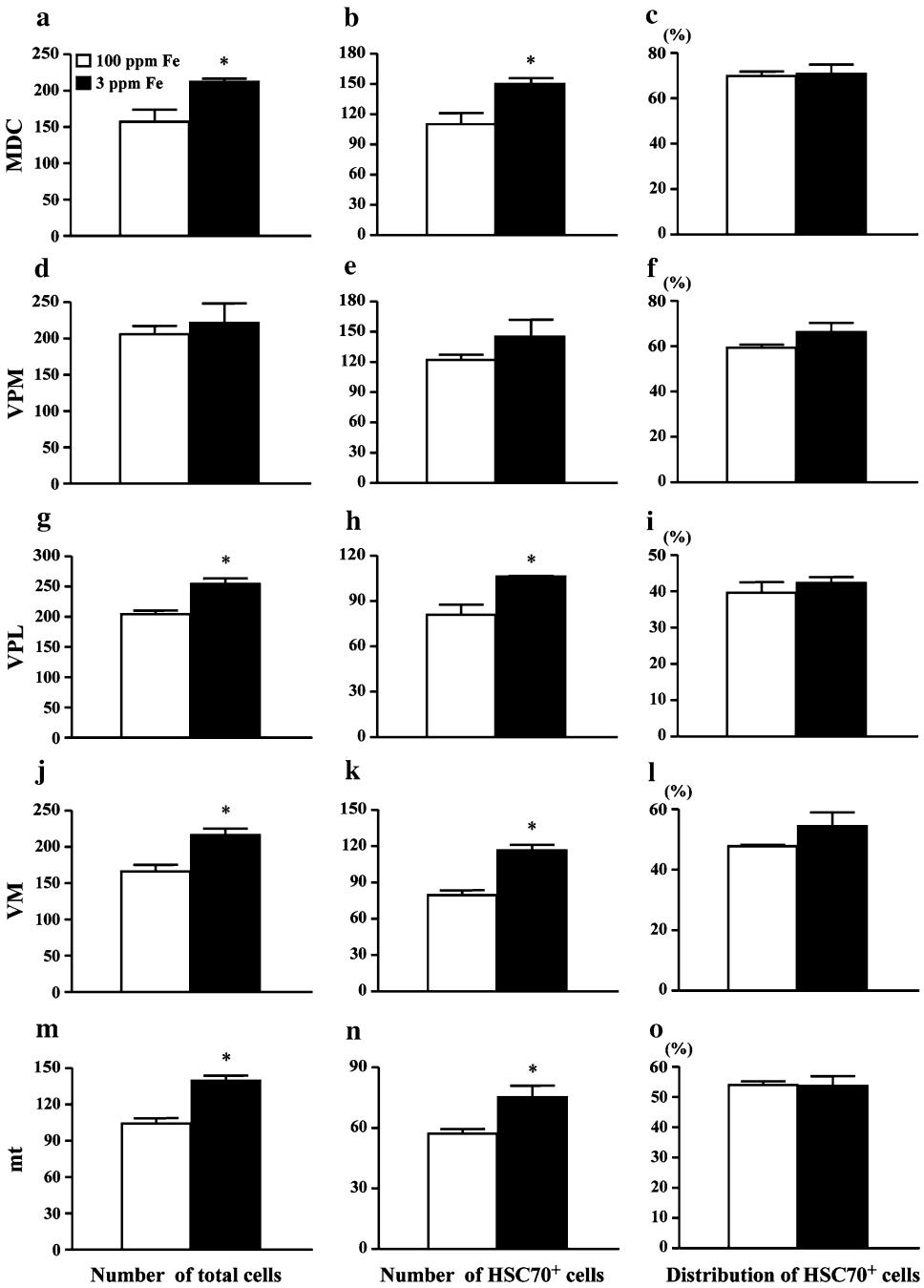

Fig. 7 The mean number of total (**a**, **d**, **g**, **j** and **m**) and HSC70-positive ($HSC70^+$; **b**, **e**, **h**, **k**, and **n**) cells counted in central mediodorsal thalamic nucleus (MDC, **a**–**c**), ventral posteromedial thalamic nucleus (VPM, **d**–**f**), ventral posterolateral thalamic nucleus (VPL, **g**–**i**), ventromedial thalamic nucleus (VM, **j**–**l**), and mammillothalamic tract (mt, **m**–**o**). The percent distribution of $HSC70^+$ cells (**c**, **f**, **i**, **l** and **o**) is also shown. Mean ± SEM. *$p < 0.05$ versus 100 ppm Fe group

between behavioral and morphological changes, in response to iron deficiency anemia.

Conclusions

The provision of a low-iron diet to newly weaned rats for 20 weeks caused severe anemia. The anemic rats showed less voluntary activity. According to the proteomic analysis of the diencephalon, greater expression of HSC70 in the iron-deficient and anemic rats was found. Although the modification of HSC70 was not affected by the iron deficiency anemia, the total expression level was greater in the iron-deficient and anemic rats. According to the results of the PLA, HSC70 was distributed in the cellular bodies and the extracellular space. A greater number of HSC70-positive cells was also observed in the diencephalon of rats fed a low-iron diet, but this change was induced in parallel with the number of total cells. Furthermore, HSC70 signals were generally noted in the extracellular space of mt, although the morphologies of the signal aggregates were different between control and iron-deficient and anemic

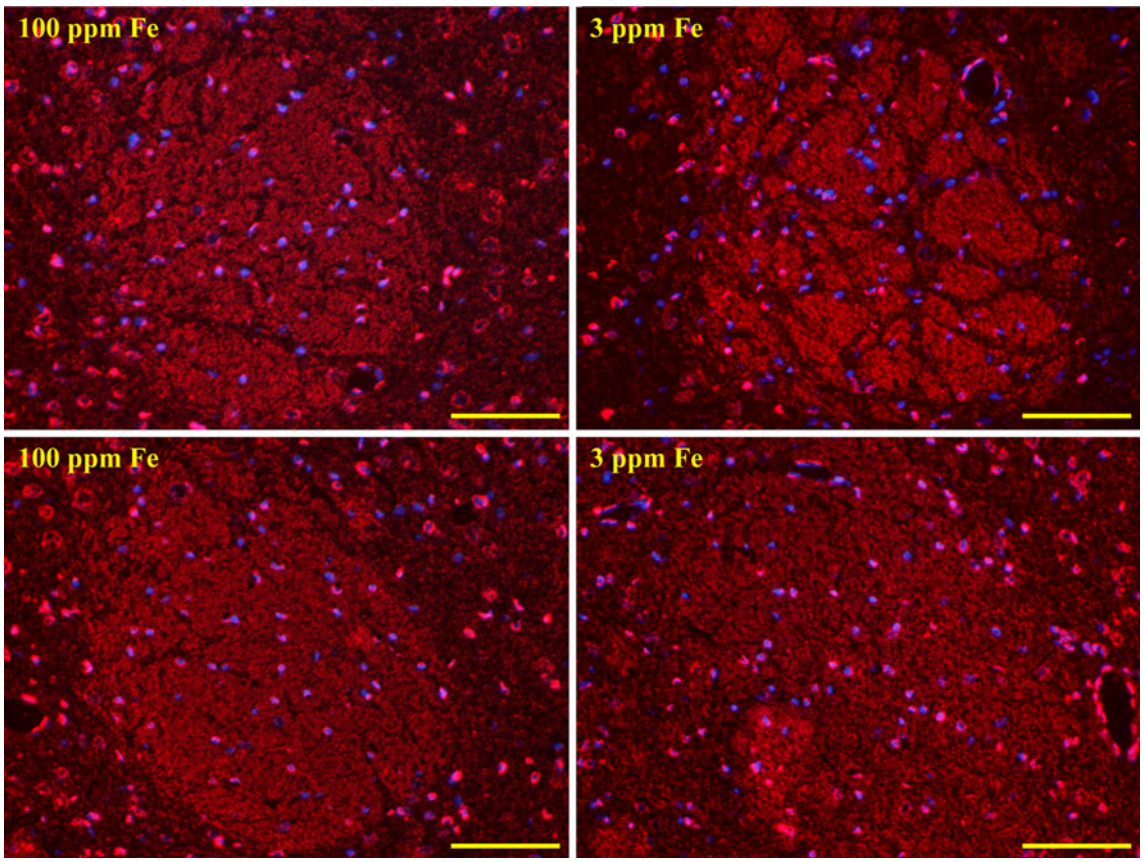

Fig. 8 Typical staining patterns of HSC70 (*red*) and nuclei (*blue*) in the mammillothalamic tract (mt). *Scale bars* 50 μm

rats. These results suggested that iron deficiency anemia caused the morphological changes in the diencephalon and might be related to the neuropathogenesis. The altered expression and distribution of HSC70 might play some role in the morphological changes.

Acknowledgments This study was supported by a Grant-in-Aid for Scientific Research S (19100009, Y.O.) and Exploratory Research (20650104, Y.O.) from the Japan Society for the Promotion of Science, and Young Scientists B (21700656, F.K.) from Ministry of Education, Culture, Sports, Science and Technology, Japan.

References

1. Edgerton VR, Ohira Y, Hettiarachchi J, Senewiratne B, Gardner GW, Barnard RJ (1981) Elevation of hemoglobin and work tolerance in iron-deficient subjects. J Nutr Sci Vitaminol (Tokyo) 27:77–86
2. Gardner GW, Edgerton VR, Senewiratne B, Barnard RJ, Ohira Y (1977) Physical work capacity and metabolic stress in subjects with iron deficiency anemia. Am J Clin Nutr 30:910–917
3. Haas JD, Brownlie TIV (2001) Iron deficiency and reduced work capacity: a critical review of the research to determine a causal relationship. J Nutr 131:676S–690S
4. Carlson ES, Magid R, Petryk A, Georgieff MK (2008) Iron deficiency alters expression of genes implicated in Alzheimer disease pathogenesis. Brain Res 1237:75–83
5. Finch CA, Miller LR, Inamdar AR, Person R, Seiler K, Mackler B (1976) Iron deficiency in the rat. Physiological and biochemical studies of muscle dysfunction. J Clin Invest 58:447–453
6. Naito Y, Tsujino T, Matsumoto M, Sakoda T, Ohyanagi M, Masuyama T (2009) Adaptive response of the heart to long-term anemia induced by iron deficiency. Am J Physiol Heart Circ Physiol 296:H585–H593
7. Ohira Y, Hegenauer J, Strause L, Chen CS, Saltman P, Beinert H (1982) Mitochondrial NADH dehydrogenase in iron-deficient and iron-repleted rat muscle: an EPR and work performance study. Br J Haematol 52:623–630
8. Perkkiö MV, Jansson LT, Henderson S, Refino C, Brooks GA, Dallman PR (1985) Work performance in the iron-deficient rat: improved endurance with exercise training. Am J Physiol 249:E306–E311
9. Tran PV, Carlson ES, Fretham SJB, Georgieff MK (2008) Early-life iron deficiency anemia alters neurotrophic factor expression and hippocampal neuron differentiation in male rats. J Nutr 138:2495–2501
10. Unger EL, Wiesinger JA, Hao L, Beard JL (2008) Dopamine D_2 receptor expression is altered by changes in cellular iron levels in PC12 cells and rat brain tissue. J Nutr 138:2487–2494
11. Rao R, Tkac I, Townsend EL, Gruetter R, Georgieff MK (2003) Perinatal iron deficiency alters the neurochemical profile of the developing rat hippocampus. J Nutr 133:3215–3221
12. Rao R, Tkac I, Townsend EL, Ennis K, Gruetter R, Georgieff MK (2007) Perinatal iron deficiency predisposes the developing rat hippocampus to greater injury from mild to moderate hypoxia-ischemia. J Cereb Blood Flow Metab 27:729–740

13. Ward KL, Tkac I, Jing Y, Felt B, Beard J, Connor J, Schallert T, Georgieff MK, Rao R (2007) Gestational and lactational iron deficiency alters the developing striatal metabolome and associated behaviors in young rats. J Nutr 137:1043–1049
14. Badaracco ME, Ortiz EH, Soto EF, Connor J, Pasquini JM (2008) Effects of transferrin on hypomyelination induced by iron deficiency. J Neurosci Res 86:2663–2673
15. Todorich B, Pasquini JM, Garcia CI, Paez PM, Connor JR (2009) Oligodendrocytes and myelination: the role of iron. Glia 57:467–478
16. Grantham-McGregor S, Ani C (2001) A review of studies on the effect of iron deficiency on cognitive development in children. J Nutr 131:649S–668S
17. Oski FA, Honig AS (1978) The effects of therapy on the developmental scores of iron-deficient infants. J Pediatr 92:21–25
18. Oski FA, Honig AS, Helu B, Howanitz P (1983) Effects of iron therapy on behavior performance in nonanemic, iron-deficient infants. Pediatrics 71:877–880
19. Beard J (2007) Recent evidence from human and animal studies regarding iron status and infant development. J Nutr 137:524S–530S
20. Lozoff B, Beard J, Connor J, Barbara F, Georgieff M, Schallert T (2006) Long-lasting neural and behavioral effects of iron deficiency in infancy. Nutr Rev 64:S34–S43
21. Lozoff B, Georgieff M (2006) Iron deficiency and brain development. Semin Pediatr Neurol 13:158–165
22. Haber S, McFarland NR (2001) The place of the thalamus in frontal cortical-basal ganglia circuits. Neuroscientist 7:315–324
23. Smith Y, Raju D, Nanda B, Pare JF, Galvan A, Wichmann T (2009) The thalamostriatal systems: anatomical and functional organization in normal and parkinsonian states. Brain Res Bull 78:60–68
24. Boikess SR, O'Dell SJ, Marshall JF (2010) A sensitizing D-amphetamine dose regimen induces long-lasting spinophilin and VGLUT1 protein upregulation in the rat diencephalon. Neurosci Lett 469:49–54
25. Floyd NS, Price JL, Ferry AT, Keay KA, Bandler R (2001) Orbitomedial prefrontal cortical projections to hypothalamus in the rat. J Comp Neurol 432:307–328
26. Sesack SR, Bunney BS (1989) Pharmacological characterization of the receptor mediating electrophysiological responses to dopamine in the rat medial prefrontal cortex: a microiontophoretic study. J Pharmacol Exp Ther 248:1323–1333
27. Sesack SR, Deutch AY, Roth RH, Bunney BS (1989) Topographical organization of the efferent projections of the medial prefrontal cortex in the rat: an anterograde tract-tracing study with *Phaseolus vulgaris* leucoagglutinin. J Comp Neurol 290:213–242
28. Gozal YM, Duong DM, Gearing M, Cheng D, Hanfelt JJ, Funderburk C, Peng J, Lah JJ, Levey AI (2009) Proteomics analysis reveals novel components in the detergent-insoluble subproteome in Alzheimer's disease. J Proteome Res 8:5069–5079
29. Reed TT, Pierce WM, Markesbery WR, Butterfield DA (2009) Proteomic identification of HNE-bound proteins in early Alzheimer disease: insights into the role of lipid peroxidation in the progression of AD. Brain Res 1274:66–76
30. Zellner M, Veitinger M, Umlauf E (2009) The role of proteomics in dementia and Alzheimer's disease. Acta Neuropathol 118:181–195
31. Basso M, Giraudo S, Corpillo D, Bergamasco B, Lopiano L, Fasano M (2004) Proteome analysis of human substantia nigra in Parkinson's disease. Proteomics 4:3943–3952
32. Leverenz JB, Umar I, Wang Q, Montine TJ, McMillan PJ, Tsuang DW, Jin J, Pan C, Shin J, Zhu D, Zhang J (2007) Proteomic identification of novel proteins in cortical Lewy bodies. Brain Pathol 17:139–145
33. Stauber J, Lemaire R, Franck J, Bonnel D, Croix D, Day R, Wisztorski M, Fournier I, Salzet M (2008) MALDI imaging of formalin-fixed paraffin-embedded tissues: application to model animals of Parkinson disease for biomarker hunting. J Proteome Res 7:969–978
34. Xia Q, Liao L, Cheng D, Duong DM, Gearing M, Lah JJ, Levey AI, Peng J (2008) Proteomic identification of novel proteins associated with Lewy bodies. Front Biosci 13:3850–3856
35. Fredriksson S, Gullberg M, Jarvius J, Olsson C, Pietras K, Gústafsdóttir SM, östman A, Landegren U (2002) Protein detection using proximity-dependent DNA ligation assays. Nat Biotechnol 20:473–477
36. Söderberg O, Gullberg M, Jarvius M, Ridderstråle K, Leuchowius KJ, Jarvius J, Wester K, Hydbring P, Bahram F, Larsson LG, Landefren U (2006) Direct observation of individual endogenous protein complexes in situ by proximity ligation. Nat Methods 12:995–1000
37. Edgerton VR, Bryant SL, Gillespie CA, Gardner GW (1972) Iron deficiency anemia and physical performance and activity of rats. J Nutr 102:381–400
38. Andringa G, Bol JGJM, Wang X, Boekel A, Bennett MC, Chase TN, Drukarch B (2006) Changed distribution pattern of the constitutive rather than the inducible HSP70 chaperone in neuromelanin-containing neurons of the Parkinsonian midbrain. Neuropathol Appl Neurobiol 32:157–169
39. Ramaglia V, Harapa GM, White N, Buck LT (2004) Bacterial infection and tissue-specific Hsp72, -73 and -90 expression in western painted turtles. Comp Biochem Physiol C 138:139–148
40. Sumitani K, Miyamoto O, Yamagami S, Okada Y, Itano T, Murakami T, Negi T (2002) The influence of severe long-term exercise on the mouse hippocampus. Nippon Seirigaku Zasshi 64:152–158
41. Chen WQ, Diao WH, Viidik A, Skalichy M, Höger H, Lubec G (2008) Modulation of the hippocampal protein machinery in voluntary and treadmill exercising rats. Biochim Biophys Acta 1784:555–562
42. Aquino DA, Peng D, Lopez C, Farooq M (1998) The constitutive heat shock protein-70 is required for optimal expression of myelin basic protein during differentiation of oligodendrocytes. Neurochem Res 23:413–420
43. Jones EG (2007) The thalamus, 2nd edn. Cambridge University Press, Cambridge
44. Kandel ER, Schwartz JH, Jessell TM (2000) Principles of neural science, 4th edn. Elsevier, New York
45. Bureau I, von Saint Paul F, Svoboda K (2006) Interdigitated paralemniscal and lemniscal pathways in the mouse barrel cortex. PLoS Biol 4:e382
46. Wimmer VC, Bruno RM, de Kock CPJ, Kuner T, Sakmann B (2010) Dimensions of a projection column and architecture of VPM and POm axons in rat vibrissal cortex. Cereb Cortex 20:2265–2276